CrossMark

Domain imaging in ferroelectric thin films via channeling-contrast backscattered electron microscopy

Jon F. Ihlefeld[1,*], Joseph R. Michael[2], Bonnie B. McKenzie[2], David A. Scrymgeour[3], Jon-Paul Maria[4], Elizabeth A. Paisley[1], and Andrew R. Kitahara[1]

[1] *Electronic, Optical and Nano Materials Department, Sandia National Laboratories, Albuquerque, NM 87185, USA*

[2] *Materials Performance and Characterization Department, Sandia National Laboratories, Albuquerque, NM 87185, USA*

[3] *Microsystems Science and Technology Center, Sandia National Laboratories, Albuquerque, NM 87185, USA*

[4] *Department of Materials Science and Engineering, North Carolina State University, Raleigh, NC 27695, USA*

ABSTRACT

Ferroelastic domain walls provide opportunities for deterministically controlling mechanical, optical, electrical, and thermal energy. Domain wall characterization in micro- and nanoscale systems, where their spacing may be of the order of 100 nm or less is presently limited to only a few techniques, such as piezoresponse force microscopy and transmission electron microscopy. These respective techniques cannot, however, independently characterize domain polarization orientation and domain wall motion in technologically relevant capacitor structures or in a non-destructive manner, thus presenting a limitation of their utility. In this work, we show how backscatter scanning electron microscopy utilizing channeling contrast yield can image the ferroelastic domain structure of ferroelectric films with domain wall spacing as narrow as 10 nm. Combined with electron backscatter diffraction to identify grain orientations, this technique provides information on domain orientation and domain wall type that cannot be readily measured using conventional non-destructive methods. In addition to grain orientation identification, this technique enables dynamic domain structure changes to be observed in functioning capacitors utilizing electrodes that are transparent to the high-energy backscattered electrons. This non-destructive, high-resolution domain imaging technique is applicable to a wide variety of ferroelectric thin films and a multitude of material systems where nanometer-scale crystallographic twin characterization is required.

Address correspondence to E-mail: jihlefe@sandia.gov

Springer

Introduction

Domain walls in ferroelectrics are crystallographic twin interfaces that provide opportunities for control of optical, electrical, mechanical, and thermal energy. For example, domain walls have been shown to possess differing electrical conductivity than neighboring domains enabling nanoscale resistive devices to be developed [1, 2]; their motion is the basis of high piezoelectric and dielectric response by providing extrinsic contributions to strain [3, 4] and permittivity [5], respectively; they can separate regions of differing optical indices and thus can be used to modulate light [6] and store optical data [7]; and can act as phonon scattering sites providing for a means to rapidly and deterministically control thermal energy [8–11]. Given the demonstrated and potential technological importance of domain walls, means to control and characterize their structure and populations is of critical importance.

Imaging domain structure in ferroelectric materials can be achieved through many techniques including optical microscopy with polarized light, scanning probe microscopy (piezoresponse force microscopy, PFM), scanning second harmonic generation, transmission electron microscopy (TEM), and even scanning electron microscopy (SEM), among others [12–14]. Some of these techniques, such as polarized optical microscopy and scanning second harmonic generation, are well suited to bulk ceramics and single crystals where domain sizes may be much larger than the wavelength of the imaging light. Imaging domain structure in thin films is more challenging owing to very fine domain sizes, which scale with thickness and/or grain size [15, 16] and preclude conventional optical approaches. For this reason, domain structure characterization in thin film ferroelectrics is conventionally done using non-destructive PFM or destructive TEM methods. For studies where non-destructive measurements are desired, PFM affords high-resolution imaging that can provide information on polarization direction, domain wall type, and piezoelectric coefficients. While PFM can provide domain orientation information, film or grain orientation must be known a priori. Therefore, for quantitative understanding of domain structure, this measurement technique must be combined with approaches that can identify grain orientations of the same grains studied by PFM.

It would be advantageous to have an imaging technique that can provide high-resolution domain structure characterization and grain orientation information. Imaging domains within an SEM equipped with an electron backscatter diffraction detector provides this capability. SEM has been utilized in a limited number of studies to image the domain structure of bulk ferroelectric single crystals [17–20] and ceramics [19, 21–24]. Several different techniques have been explored, including secondary electron imaging utilizing electron channeling [17, 19], secondary electron imaging where contrast is provided by differing polarization charge or work function affecting electron yield [20], electron beam stimulated polarization currents [19], electron backscatter diffraction (EBSD) [24], and backscatter electron imaging utilizing electron channeling [21, 23]. A simple and high-resolution approach is to utilize a backscatter electron (BSE) imaging mode where the channeling of incident electrons within domains of different orientations modulates the backscatter yield and provides a crystallographically sensitive contrast mechanism. This method has been used on bulk materials and has been shown to allow imaging of domains with widths as small as 30 nm [21]. With a few exceptions, however, this approach has not been widely applied to the imaging of domains in thin film samples [11, 25]. In the present work, we will show how backscatter scanning electron microscopy can be used to image the ferroelastic domain structure of polycrystalline bilayer lead zirconate titanate (PZT) thin films and an epitaxial PZT film. Samples studied include (1) A 170-nm-thick bilayer PZT film with a $PbZr_{0.2}Ti_{0.8}O_3$ layer on top of a $PbZr_{0.7}Ti_{0.3}O_3$ layer (denoted as 20/80–70/30). This sample was used to assess the impact of imaging conditions on resolution, to compare SEM and PFM imaging, and to show how SEM and EBSD can complement PFM data. (2) A 230-nm-thick bilayer PZT film with a $PbZr_{0.3}Ti_{0.7}O_3$ layer on top of a $PbZr_{0.7}Ti_{0.3}O_3$ layer (denoted as 30/70–70/30), which was used to demonstrate how backscatter SEM imaging could be used monitor domain structure changes in an electrode/ferroelectric/electrode structure while electric fields are applied. (3) A 160–nm-thick epitaxial $PbZr_{0.2}Ti_{0.8}O_3$ thin film, which was used to demonstrate domain imaging with high spatial resolution. Bilayers, owing to the ability to prepare large grained samples (>500 nm) with high densities of finely spaced ferroelastic domain walls

that are mobile under applied electric fields [26–28], provide an opportunity to assess the resolution performance of backscatter electron imaging of domains and demonstrate domain imaging while electric fields are applied. The bilayer structures used in this work consists of a ~60–nm-thick zirconium-rich ($PbZr_{0.7}Ti_{0.3}O_3$) layer in contact with a platinum bottom electrode and a titanium-rich ($PbZr_{0.2}Ti_{0.8}O_3$ or $PbZr_{0.3}Ti_{0.7}O_3$) layer on top. The titanium-rich layer possesses a high density of 90° ferroelastic domain walls.

Experimental procedures

All scanning electron microscopy experiments were performed within a Zeiss Supra 55VP instrument. Backscatter electron microscopy images were collected with acceleration voltages ranging from 10 to 20 kV with a solid state, KE Development LTD, Four Quadrant Backscattered Electron Type 211 detector. Working distances of less than 6 mm were used. This working distance denotes the distance between the sample surface and the pole-piece, not the backscatter detector, which is located between the pole-piece and the sample. EBSD was conducted in the Zeiss Supra 55VP SEM utilizing an Oxford EBSD system consisting of Flamenco collection software and a Nordlys II EBSD detector. The EBSD patterns were indexed with respect to the unit cell of $PbZr_{0.2}Ti_{0.8}O_3$ with $P4mm$ crystal symmetry and lattice parameters of 3.953 and 4.148 Å. Patterns were obtained with a beam current of 5 nA and an accelerating voltage of 20 kV. The resulting orientation data were analyzed with the Oxford Channel 5 software package. In order to better visualize the inverse pole figure maps, some data cleaning consisting of 8 nearest neighbor hole filling was used.

PFM imaging was performed with a Digital Instruments Dimension 3100 atomic force microscope using sharp, <20 nm, platinum-coated tips (DPER-XSC11 MikroMasch) with a nominal resonance frequency of 12–18 kHz. PFM images were collected near the cantilever's in-contact resonance frequency to enhance the lateral resolution. The imaging signal of 2.5 V_{peak} voltage at ~58 kHz was provided by an external function generator. The out-of-plane (vertical PFM) signals were collected. All PFM data presented are the X data channel ($R \times \cos \theta$ image) in uncalibrated units. The phase was adjusted to minimize the data in the Y channel.

Bilayer PZT films were prepared using chemical solution deposition employing an inverted mixing order solution chemistry [29] with titanium isopropoxide, zirconium butoxide (80 wt% in butanol), lead (IV) acetate, glacial acetic acid, and methanol as the precursor chemicals for the bilayer films. Titanium isopropoxide was added to zirconium butoxide and allowed to stir for 5 min. This solution was chelated with acetic acid and allowed to stir for 5 min prior to the addition of methanol. Lead (IV) acetate was added and the solution was heated to 90 °C until dissolution of the acetate and a clear solution resulted. Sequential doses of methanol and acetic acid were added while cooling to room temperature resulting in a 0.35 M solution. Bilayer films were spin cast onto 100 nm Pt/40 nm ZnO/400 nm SiO_2/silicon substrates whose preparation is discussed elsewhere [30]. Films were cast at 4000 RPM for 30 s. The zirconium-rich solution was first deposited followed by a hotplate pyrolysis at 450 °C for 1 min. The titanium-rich solution was then spin cast followed by sequential hotplate pyrolysis steps of 300 and 450 °C, each for 1 min. One to two additional titanium-rich layers were deposited and pyrolyzed and the films were then annealed in a preheated furnace at 700 °C for 10 min. The epitaxial film was prepared by pulsed laser deposition (PLD) onto a 100-nm-thick $SrRuO_3$ epilayer on a (001)-oriented $SrTiO_3$ substrate. The $SrRuO_3$ epilayer was prepared via 30° off-axis RF magnetron sputtering. A 75-mm diameter $SrRuO_3$ target 75 W in 20 mTorr of a 5:1 $Ar:O_2$ atmosphere onto a (001)-oriented $SrTiO_3$ substrate. A substrate platen temperature of 610 °C was used as monitored by a thermocouple located near the platen. The 160-nm-thick PZT film was deposited with the following conditions: 200 mTorr oxygen, a 150 mJ KrF beam, 12 mm^2 spot size, a target-to-substrate separation of 6.5 cm, and a 15 Hz laser repetition rate.

A photoresist lift off technique and platinum pads were used to provide for fiducial markings to enable electron and scanning probe microscopy measurements to be performed in the same region on the 20/80–70/30 bilayer and epitaxial samples. Imaging under an applied electric field was performed on a 30/70–70/30 bilayer sample and was achieved by preparing 90-nm-thick 500 × 500 µm platinum pads through a shadow mask by RF magnetron sputtering. The mask was then offset by ~300 µm and a 3-nm-thick platinum film deposited. To provide a platform allowing electric fields to be supplied to the sample

during imaging, the bilayer film was mounted to a silicon wafer with silver paint. Gold wire was then bonded to the ∼90-nm-thick pads using silver epoxy (EPO-TEK H20E) and to thicker wire epoxied to alumina insulating pads adhered to the silicon wafer. Electrical feedthroughs on the microscope were used to supply a voltage to the sample. Three 3-volt lithium ion batteries were used in series to apply ±9 V across the film. Continuity of the 3-nm-thick platinum layer was verified by capacitance measurements of the bilayer film.

Results and discussion

An initial experiment was performed using a 20/80–70/30 bilayer sample to identify necessary conditions to observe the fine domain structure present in thin films. The film was imaged with 10, 15, and 20 kV acceleration voltages at working distances of 4.5 and 5.3 mm, with the results shown in Fig. 1. All images possess features that are consistent with stripe domain features. However, the greatest clarity of these features is observed for 15 and 20 kV

acceleration voltages, as indicated by the arrows in Fig. 1b. These arrows highlight domains that are clearly observed using 15 and 20 kV conditions, but are not observed with 10 kV acceleration voltages. Additionally, resolution of stripe domain features is improved by decreasing the working distance from 5.3 to 4.5 mm. Arrows in Fig. 1c show domains that are resolved with a 4.5 mm working distance, but are not well resolved with a 5.3 mm working distance (Fig. 1f). Increased resolution with increased beam energy can be understood by a greater beam energy resulting in a smaller probe size and deeper interaction volumes. Increased resolution with smaller working distances results from increased solid angle of the scanning beam and also increased solid angle of backscattered electron detection. Based on the results of this initial study, the images collected in the remainder of this work utilized working distances less than 5 mm and accelerating voltages of 20 kV.

With the necessary conditions for high-resolution imaging established, Fig. 2 shows images of the 20/80–70/30 bilayer in a region that was also measured by PFM. Stripe domain structures are clearly observed in many grains in the overall image in
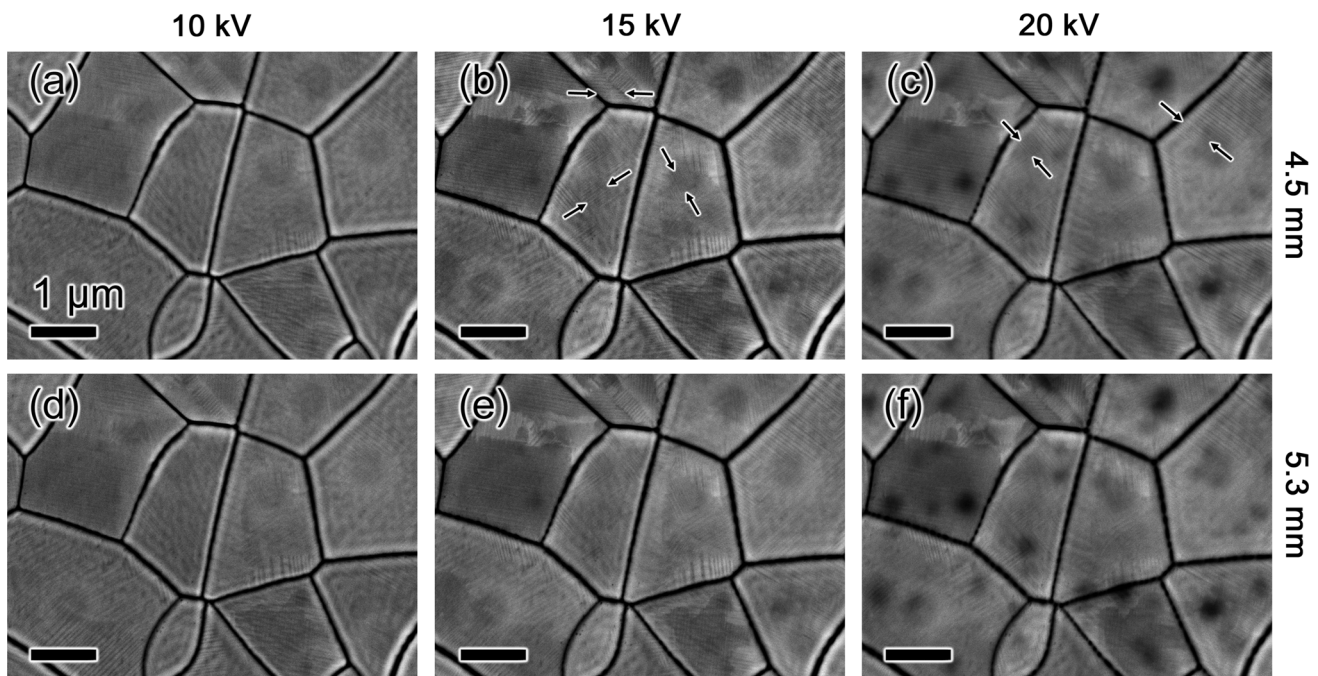

Figure 1 Backscattered electron micrographs of a $PbZr_{0.2}Ti_{0.8}O_3$/ $PbZr_{0.7}Ti_{0.3}O_3$ bilayer film under 10 kV accelerating voltage (**a**, **d**), 15 kV accelerating voltage (**b**, **e**), and 20 kV accelerating voltage (**c**, **f**) with working distances of 4.5 mm (**a–c**) and 5.3 mm (**d–f**). *Arrows* in (**b**) indicate domains resolved with 15 and 20 kV beam energies, but not resolved at 10 kV. *Arrows* in (**c**) indicate domains resolved with a 4.5 mm working distance but not resolved with a 5.3 mm working distance. Changes in the levels and gamma values were independently performed for each image to represent similar brightness and contrast.
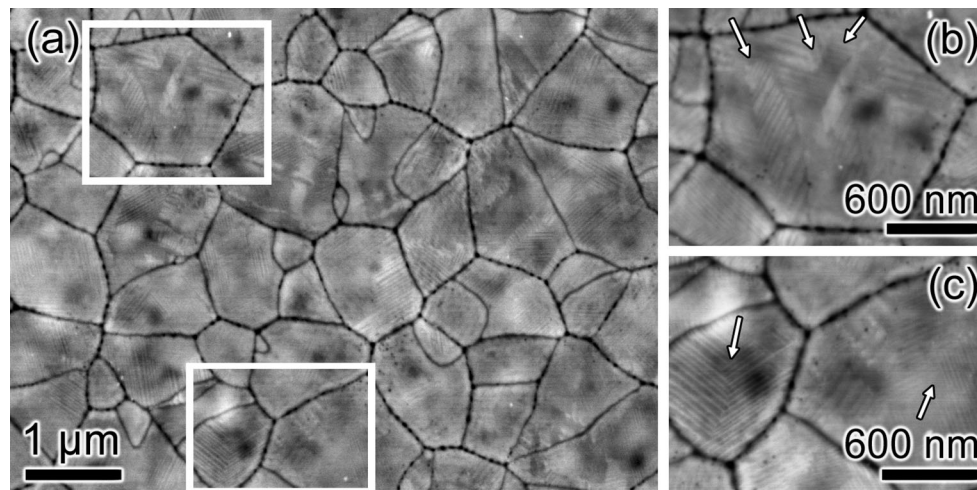
Figure 2 Backscattered electron micrographs of a $PbZr_{0.2}Ti_{0.8}O_3/PbZr_{0.7}Ti_{0.3}O_3$ bilayer film imaged with a 20 kV electron accelerating voltage. **a** shows an overview scan and **b**, **c** show higher magnification images of the top and bottom *boxes* in (**a**). *Arrows* in Fig. 2a. (**b**) and (**c**) identify domains that are observed in the PFM images of Fig. 3. A change in the levels from 0–256 to 0–185 and gamma value to 1.15 was performed to increase contrast in the image.

Fig. 2a. Figure 2b, c highlight two specific regions where distinct domain structure can be observed. The grain in the center of Fig. 2b has a complex domain structure with bundles of stripe domains highlighted with arrows that are similar to those observed by Ivry et al. using PFM [25]. These domain bundles almost certainly form to minimize strain and polarization fields. The grains highlighted in Fig. 2c show regions of intersecting stripe domains (white arrows). In measuring the distances between the stipe domains in Fig. 2c, we observe that domains spaced as narrowly as ~21 nm are clearly resolved, which is of the same order as that observed for bulk ceramic samples using a similar technique [21]. As will be shown with the epitaxial film later, this value does not necessarily represent a fundamental resolution limit; rather it reflects the finest resolved spacing of domains present in this particular region of the sample.

Figure 3 shows topographic atomic force microscopy (Fig. 3a, d) and out-of-plane PFM images (Fig. 3b–f) for the regions imaged by BSE in Fig. 2b and c. The domain structure was imaged in a pre-poled state (Fig. 3b, e, respectively) and after the application of +8 volts using the scanning probe (Fig. 3c, f), which we denote as the poled state. The BSE images (Fig. 2b, c) were collected after PFM poling. In Fig. 3c, we clearly see domain bundle structures that correspond to the same features observed in Fig. 2b (arrows identify the domain bundles). In Fig. 3f, we can identify the intersection

of stripe domains in the left-most grain and the complex domain structure of the right-most grain; both features are also observed in Fig. 2c. The domain spacing within the same grain measured by the BSE technique in Fig. 2c is identical at ~21 nm. This data clearly show that BSE imaging may be used to gather similar domain morphology information as PFM, with similar resolution.

The BSE and PFM data allow domain structure to be imaged, but because randomly oriented polycrystalline grains comprise these films, information about crystallographic relations cannot be obtained. To obtain these data on these same films, EBSD was employed in the same region. Figure 4a shows an EBSD inverse pole figure orientation (IPF) map with respect to the sample normal for the same region as shown in Fig. 2, with the same highlighted regions identified by the white boxes. The fine domain structure combined with carbon contamination from SEM imaging results in some pixels that are difficult to assign; however, we can identify orientations for most grains in the imaged area. No overall preferential orientation can be deduced from these data, demonstrating that this film consists of randomly oriented grains. Additionally, EBSD has suitable resolution to enable identification of some specific domain regions. Focusing on the grain imaged in Fig. 2b, which is the topmost highlighted grain in Fig. 4a, we can identify the domain bundle structure observed in both BSE and PFM as the alternating
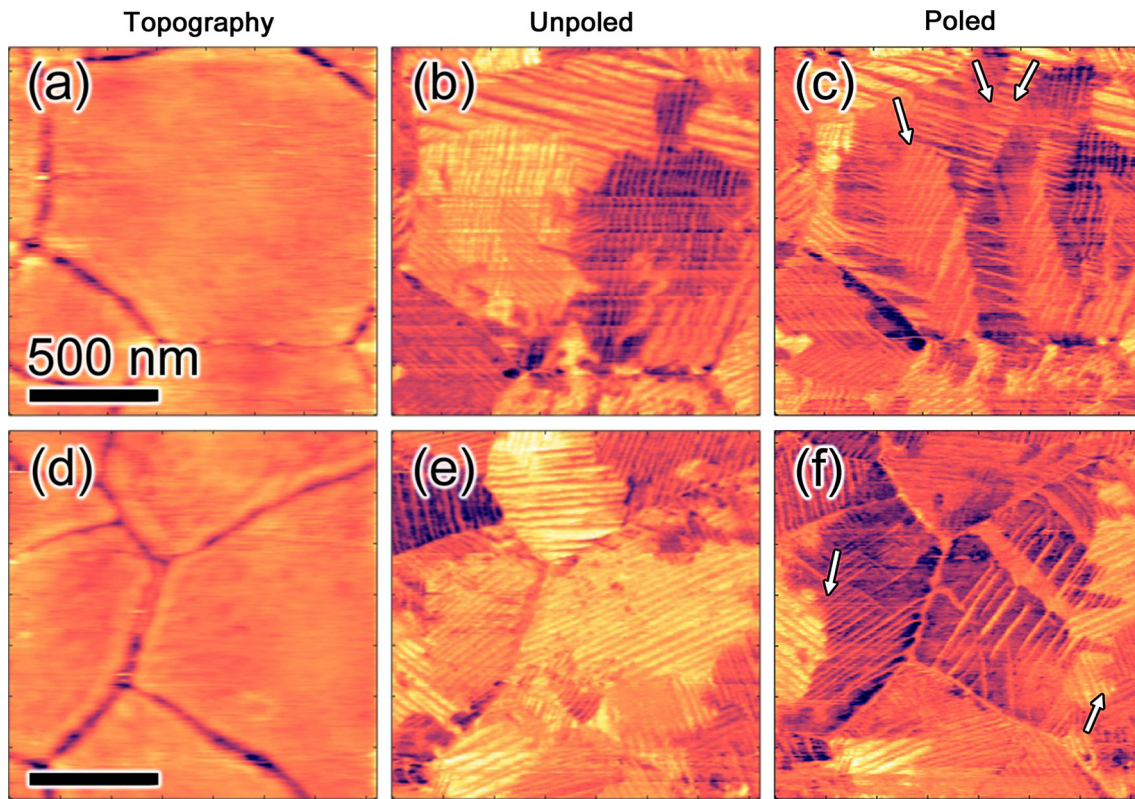
Figure 3 Scanning probe microscopy images of the regions highlighted in Fig. 2b (*top row*) and c (*bottom row*). **a, d** are topographic scans of the respective regions. **b, e** are piezoresponse force micrographs in the unpoled state, and **c, f** are piezoresponse force micrographs in the poled state. *Arrows* in (**c**) and (**f**) identify domains that are observed in Fig. 2.

Figure 4 a Inverse pole figure (IPF) map with respect to the sample surface normal of the region shown in Fig. 2a. The *inset* shows the color key used for the IPF corresponding to the map in (**a**). **b, c** show the <001> pole figures from the grains highlighted in Fig. 2b, c, respectively.
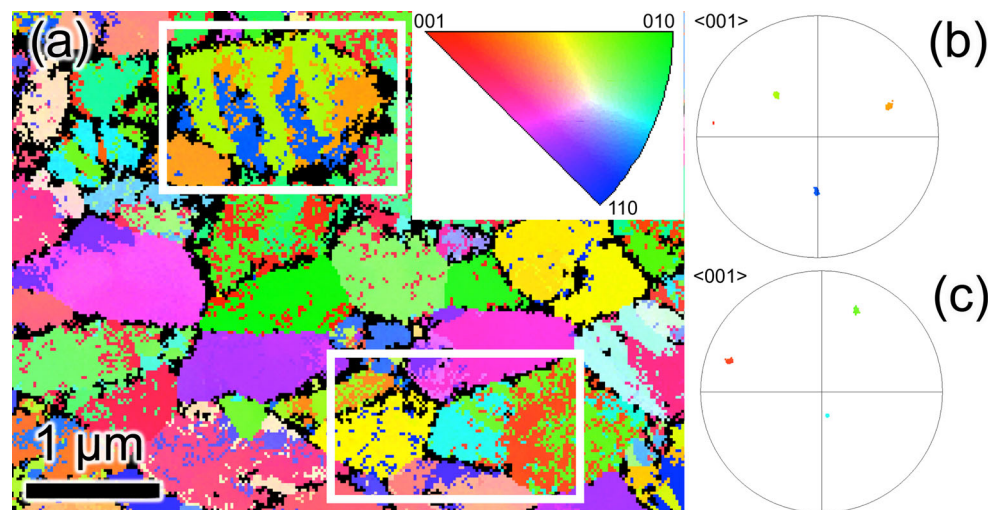
blue/green stripes. This particular grain has an orientation close to <011> out-of-plane. Using pole figure analysis on this grain (Fig. 4b), showing the <001> polar axes in tetragonal PZT, we can see that these regions are separated by 90°. This observation demonstrates the utility of the combined BSE and

EBSD technique to identify and image the ferroelastic domain structure in the 20/80 layer of the randomly oriented bilayer film. Furthermore, it can be seen that these polar axes are oriented by approximately 50 and 65° from the surface normal. Likewise, for the right-most grain highlighted in the lower box (the
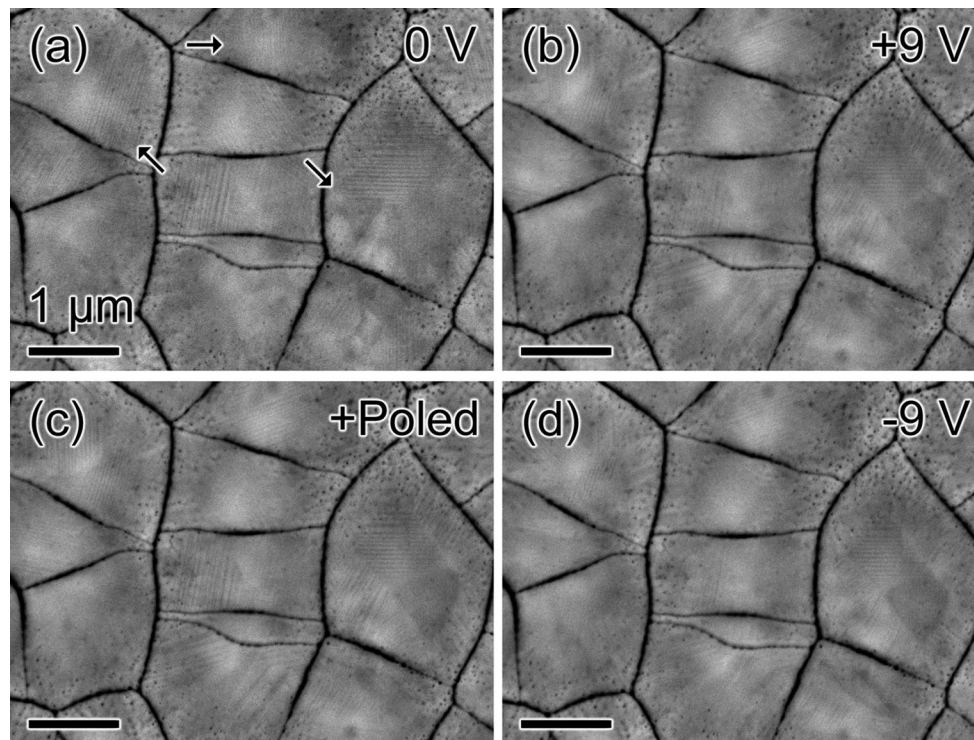
Figure 5 *in operando* backscatter electron micrographs of a PbZr$_{0.3}$Ti$_{0.7}$O$_3$/PbZr$_{0.7}$Ti$_{0.3}$O$_3$ bilayer film imaged through a 3-nm-thick platinum electrode, **a** shows a micrograph in the unpoled state, **b** shows the same region with 9 V across the film, **c** is after removal of the 9 V applied bias in the positive poled state, and **d** is with −9 V applied across the bilayer film. *Arrows* in (**a**) indicate regions where there are distinct changes in the domain structure in the various electrical conditions. A change in the levels from 0–256 to 0–139 and gamma value to 0.55 was performed to increase contrast in the images.

same grain as highlighted in Fig. 2c), which has an orientation near <001>, regions of differing domain orientations can be identified. Pole figure analysis for this grain is shown Fig. 4c for the <001> poles. Again, 90° angles are observed between the three <001> poles, demonstrating that these domains are separated by ferroelastic domain walls in a single grain. The polarization axes in this grain form angles of approximately 27 and 73° with the surface normal. This specific orientation information would be difficult, if not impossible, to determine from PFM data alone.

For another test of the utility of the BSE technique for imaging domains in ferroelectric thin films, *in operando* monitoring of the domain structure in a capacitor structure has been investigated. Several groups have performed PFM imaging through thin metallic electrodes; however, most efforts have focused on observing 180° ferroelectric domain structure and not ferroelastic structure [31–36]. While the metal electrode is known to reduce PFM imaging resolution [33, 37], 10 nm 180° polarization-reversal

features have been reported as resolved via this technique [32]. This notwithstanding, studies of ferroelastic domain structure through a metal electrode using PFM appear to be limited. A technique using electron channeling, such as BSE, will work so long as the electrode is sufficiently thin to allow for transparency to backscattered electrons. In this study, ferroelastic domain structure was imaged through a 3-nm-thick platinum electrode. Figure 5 shows sequential BSE images captured under conditions of (a) no applied field in an unpoled state, (b) positive 9 volts applied (i.e., positive bias to the top electrode and negative to the bottom electrode), (c) the positive remanent state, and (d) under application of negative 9 volts. Changes in the domain structure are unambiguously observed in several grains that are highlighted by arrows. To better illustrate the changes in domain structure, Fig. 6 shows two selected grains with false color applied with an inverted color profile and arrows denoting the direction of stripe domains. Changes in domain orientation while the field is applied are observed in multiple regions of each
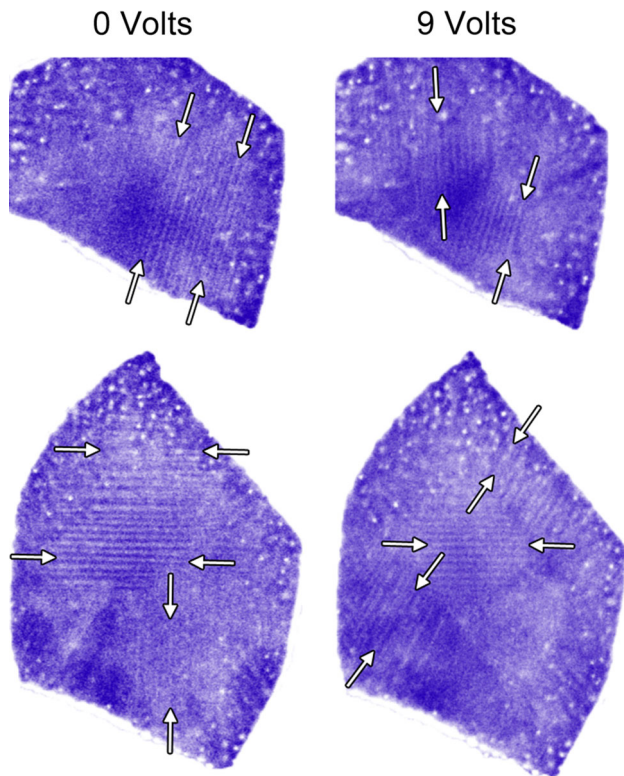
0 Volts   9 Volts

Figure 6 *In operando* backscatter electron micrographs of two specific grains from Fig. 5. The *left side* shows the grains in the unpoled state. The *right side* shows the same grains with 9 V applied across the bilayer films. *Arrows* indicate the directions of stripe domains under the different applied voltage conditions. A false color and inverted color profile have been used to accentuate the domain structure.

grain. Additionally, focusing on the top grain in Fig. 6, even with the thin platinum electrode present, stripe domains spaced as narrow as 34 nm can be resolved, demonstrating that finely spaced features can be obtained when imaging through the 3-nm-thick platinum electrode. It should be noted that the large penetration depth (the estimated Kanaya–Okayama range [38] is >1.8 μm for PZT with a 20 kV beam accelerating voltage) and low current (∼5 nA) of the scanning beam is not expected to significantly affect the performance of the capacitor or lead to changes in the domain structure. No changes in the domain structure are observed with subsequent scans, which support this notion.

Given the ubiquity of epitaxial ferroelectric thin films for the study of domain walls and domain wall properties, it was prudent to investigate the utility of the BSE technique for imaging domains of such samples. Figure 7 shows a PFM image and BSE image of the epitaxial PZT film measured in the same location. Image registry was used to correct for a slight distortion in the PFM image and enables the same domains measured with each technique to be identified with the white arrows. Regions of intersecting 90° ferroelastic domains are clearly observed in both images, and in some regions more domains are visible in the BSE data than in the PFM data. For example, for the horizontal white arrows in Fig. 7, three-stacked horizontal stripe domains are clearly visible in the BSE image, but it is difficult to resolve these in the PFM data. Since strain-
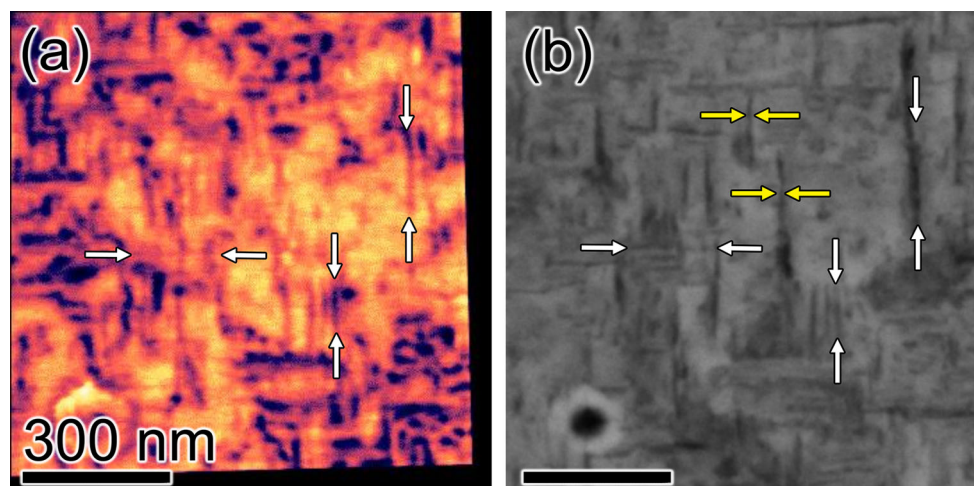

Figure 7 **a** *X*-channel PFM image and **b** backscatter electron micrograph of an epitaxial $PbZr_{0.2}Ti_{0.8}O_3$ film prepared on a (001)-oriented $SrRuO_3/SrTiO_3$ substrate. *White arrows* indicate the same domains measured in the PFM and SEM images. The

yellow arrows in (**b**) indicate the narrowest resolved domains in the image, which are ∼10 nm across. Image registry was used to identify like features and correct distortion in the PFM image.

relaxed epitaxial tetragonal PZT films on $SrTiO_3$ substrates are known to support extremely narrow ferroelastic domains [39], this sample provides a test for the resolution limits of the BSE technique for imaging ferroelastic domains. The yellow arrows in Fig. 7b highlight domains that are just 10 nm wide, indicating that the channeling-contrast BSE technique is capable of imaging extremely fine features—of the same size scale that is possible with state-of-the-art PFM approaches [40].

Finally, it is advisable to mention that this BSE technique is well suited for imaging ferroelastic domain walls in ferroelectric films where a conducting path exists for the incident electrons. For example, the platinum bottom electrode and semiconducting silicon substrate of the bilayer structures enable imaging without significant artifacts due to charging. Likewise, an exposed region of the $SrRuO_3$ conductive electrode was used to electrically contact the SEM stage for the epitaxial film, thus minimizing charging. Resolving very fine features using the BSE technique on samples devoid of a conductive bottom contact would be more challenging and may require conductive coatings to dissipate charge. For samples with conductive electrodes, this technique provides for non-destructive imaging of ferroelastic domain walls in large grained polycrystalline and epitaxial thin films in a complementary manner to widely used scanning probe methods.

Conclusion

In summary, a non-destructive backscatter electron microscopy approach using electron channeling is shown to be an effective technique for imaging ferroelastic domain structure in ferroelectric films. Nearly identical domain structure images to those collected using PFM have been obtained. Through the use of EBSD on the same region scanned using BSE, grain and domain orientations can be identified, which would not be possible using PFM methods. The technique is shown to be usable for imaging through thin electrodes and observing domain structure changes of a functioning thin film capacitor *in operando*. Finally, domains as small as 10 nm have been imaged in an epitaxial film prepared on a single crystalline substrate proving this approach to be a viable alternative to PFM for determining domain structure. The BSE technique, in combination with

EBSD, provides a platform enabling nanometer-scale twin boundary crystallographic characterization in a non-destructive manner.

Compliance with ethical standards

Conflict of Interest The authors declare that they have no conflict of interest.

References

[1] Seidel J, Martin LW, He Q, Zhan Q, Chu YH, Rother A, Hawkridge ME, Maksymovych P, Yu P, Gajek M, Balke N, Kalinin SV, Gemming S, Wang F, Catalan G, Scott JF, Spaldin NA, Orenstein J, Ramesh R (2009) Conduction at domain walls in oxide multiferroics. Nat Mater 8:229–234

[2] Guyonnet J, Gaponenko I, Gariglio S, Paruch P (2011) Conduction at domain walls in insulating $Pb(Zr_{0.2}Ti_{0.8})O_3$ thin films. Adv Mater 23:5377–5382

[3] Damjanovic D, Demartin M (1997) Contribution of the irreversible displacement of domain walls to the piezoelectric effect in barium titanate and lead zirconate titanate ceramics. J. Phys Condens Mat 9:4943–4953

[4] Zhang QM, Wang H, Kim N, Cross LE (1994) Direct evaluation of domain-wall and intrinsic contributions to the dielectric and piezoelectric response and their temperature dependence on lead zirconate-titanate ceramics. J Appl Phys 75:454

[5] Arlt G, Hennings D, de With G (1985) Dielectric-properties of fine-grained barium-titanate ceramics. J Appl Phys 58:1619–1625

[6] Land CE, Thacher PD (1969) Ferroelectric ceramic electrooptic materials and devices. P. IEEE 57:751–768

[7] Land CE, Peercy PS (1977) Photo-Ferroelectric image storage in PLZT ceramics. Inf Disp 13:20–23

[8] Mante AJH, Volger J (1971) Phonon transport in barium titanate. Physica 52:577–604

[9] Weilert MA, Msall ME, Anderson AC, Wolfe JP (1993) Phonon scattering from ferroelectric domain walls: phonon imaging in KDP. Phys Rev Lett 71:735–738

[10] Hopkins PE, Adamo C, Ye LH, Huey BD, Lee SR, Schlom DG, Ihlefeld JF (2013) Effects of coherent ferroelastic domain walls on the thermal conductivity and Kapitza conductance in bismuth ferrite. Appl Phys Lett 102:121903

[11] Ihlefeld JF, Foley BM, Scrymgeour DA, Michael JR, McKenzie BB, Medlin DL, Wallace M, Trolier-McKinstry S, Hopkins PE (2015) Room-temperature voltage tunable phonon thermal conductivity via reconfigurable interfaces in ferroelectric thin films. Nano Lett 15:1791–1795

[12] Soergel E (2005) Visualization of ferroelectric domains in bulk single crystals. Appl Phys B 81:729–751

[13] Potnis PR, Tsou NT, Huber JE (2011) A review of domain modelling and domain imaging techniques in ferroelectric crystals. Materials 4:417–447

[14] Denev SA, Lummen TTA, Barnes E, Kumar A, Gopalan V (2011) Probing ferroelectrics using optical second harmonic generation. J Am Ceram Soc 94:2699–2727

[15] Streiffer SK, Eastman JA, Fong DD, Thompson C, Munkholm A, Murty MVR, Auciello O, Bai GR, Stephenson GB (2002) Observation of nanoscale 180 degrees stripe domains in ferroelectric PbTiO$_3$ thin films. Phys Rev Lett 89:067601

[16] Catalan G, Bea H, Fusil S, Bibes M, Paruch P, Barthelemy A, Scott JF (2008) Fractal dimension and size scaling of domains in thin films of multiferroic BiFeO$_3$. Phys Rev Lett 100:027602

[17] Ikeda S, Uchikawa Y (1980) SEM imaging of ferroelectric domains. J Electron Microsc 29:209–217

[18] Zhu SN, Cao WW (1997) Direct observation of ferroelectric domains in LiTaO$_3$ using environmental scanning electron microscopy. Phys Rev Lett 79:2558–2561

[19] Sogr AA, Kopylova IB (1997) Observation of the domain structure of ferroelectrics with the scanning electron microscope. Ferroelectrics 191:401–406

[20] Le Bihan R (1989) Study of ferroelectric and ferroelastic domain structures by scanning electron microscopy. Ferroelectrics 97:19–46

[21] Gruner D, Shen ZJ (2010) Direct scanning electron microscopy imaging of ferroelectric domains after ion milling. J Am Ceram Soc 93:48–50

[22] Omori M, Mishima T, Fujimoto T (2011) Modes of domain wall motion and polarization of lead zirconate titanate polycrystals. Jpn J Appl Phys 50:09NC03

[23] Reichmann A, Zankel A, Reingruber H, Polt P, Reichmann K (2011) Direct observation of ferroelectric domain formation by environmental scanning electron microscopy. J Eur Ceram Soc 31:2939–2942

[24] Howell JA, Vaudin MD, Cook RF (2014) Orientation, stress, and strain in an (001) barium titanate single crystal with 90° lamellar domains determined using electron backscatter diffraction. J Mater Sci 49:2213–2224. doi:10.1007/s10853-013-7915-3

[25] Ivry Y, Chu DP, Durkan C (2010) Bundles of polytwins as meta-elastic domains in the thin polycrystalline simple multi-ferroic system PZT. Nanotechnology 21:065702

[26] Anbusathaiah V, Kan D, Kartawidjaja FC, Mahjoub R, Arredondo MA, Wicks S, Takeuchi I, Wang J, Nagarajan V (2009) Labile ferroelastic nanodomains in bilayered ferroelectric thin films. Adv Mater 21:3497–3502

[27] Anbusathaiah V, Jesse S, Arredondo MA, Kartawidjaja FC, Ovchinnikov OS, Wang J, Kalinin SV, Nagarajan V (2010) Ferroelastic domain wall dynamics in ferroelectric bilayers. Acta Mater 58:5316–5325

[28] Ehara Y, Yasui S, Nagata J, Kan D, Anbusathaiah V, Yamada T, Sakata O, Funakubo H, Nagarajan V (2011) Ultrafast switching of ferroelastic nanodomains in bilayered ferroelectric thin films. Appl Phys Lett 99:182906

[29] Assink RA, Schwartz RW (1993) H–1 and C–13 NMR investigations of Pb(Zr, Ti)O$_3$ thin-film precursor solutions. Chem Mater 5:511–517

[30] Shelton CT, Kotula PG, Brennecka GL, Lam PG, Meyer KE, Maria J-P, Gibbons BJ, Ihlefeld JF (2012) Chemically homogeneous complex oxide thin films via improved substrate metallization. Adv Funct Mater 22:2295–2302

[31] Gruverman A, Rodriguez BJ, Kingon AI, Nemanich RJ, Cross JS, Tsukada M (2003) Spatial inhomogeneity of imprint and switching behavior in ferroelectric capacitors. Appl Phys Lett 82:3071–3073

[32] Kim DJ, Jo JY, Kim TH, Yang SM, Chen B, Kim YS, Noh TW (2007) Observation of inhomogeneous domain nucleation in epitaxial Pb(Zr, Ti)O$_3$ capacitors. Appl Phys Lett 91:132903

[33] Jungk T, Hoffmann A, Soergel E (2007) Impact of elasticity on the piezoresponse of adjacent ferroelectric domains investigated by scanning force microscopy. J Appl Phys 102:084102

[34] Kim Y, Lu XL, Jesse S, Hesse D, Alexe M, Kalinin SV (2013) Universality of polarization switching dynamics in ferroelectric capacitors revealed by 5d piezoresponse force microscopy. Adv Funct Mater 23:3971–3979

[35] Yang SM, Kim TH, Yoon JG, Noh TW (2012) Nanoscale observation of time-dependent domain wall pinning as the origin of polarization fatigue. Adv Funct Mater 22:2310–2317

[36] Gruverman A, Wu D, Scott JF (2008) Piezoresponse force microscopy studies of switching behavior of ferroelectric capacitors on a 100-ns time scale. Phys Rev Lett 100:097601

[37] Balke N, Bdikin I, Kalinin SV, Kholkin AL (2009) Electromechanical imaging and spectroscopy of ferroelectric and piezoelectric materials: state of the art and prospects for the future. J Am Ceram Soc 92:1629–1647

[38] Kanaya K, Okayama S (1972) Penetration and energy-loss theory of electrons in solid targets. J Phys D 5:43

[39] Nagarajan V, Roytburd A, Stanishevsky A, Prasertchoung S, Zhao T, Chen L, Melngailis J, Auciello O, Ramesh R (2003) Dynamics of ferroelastic domains in ferroelectric thin films. Nat Mater 2:43–47

[40] Mtebwa M, Feigl L, Yudin P, McGilly LJ, Shapovalov K, Tagantsev AK, Setter N (2015) Room temperature concurrent formation of ultra-dense arrays of ferroelectric domain walls. Appl Phys Lett 107:142903